Physics Letters B 693 (2010) 448–451

Contents lists available at ScienceDirect

Physics Letters B

www.elsevier.com/locate/physletb

Influence of the halo upon angular distributions for elastic scattering and breakup

P. Capel [a,b,*,1], M.S. Hussein [c], D. Baye [b]

[a] National Superconducting Cyclotron Laboratory, Michigan State University, East Lansing, MI 48824, USA
[b] Physique Quantique, CP 165/82, and Physique Nucléaire Théorique et Physique Mathématique, CP229, Université Libre de Bruxelles (ULB), B-1050 Brussels, Belgium
[c] Instituto de Física, Universidade de São Paulo C.P. 66318, 05315-970 São Paulo, S.P., Brazil

ARTICLE INFO

Article history:
Received 10 August 2010
Received in revised form 24 August 2010
Accepted 27 August 2010
Available online 6 September 2010
Editor: W. Haxton

Keywords:
Halo nuclei
Elastic scattering
Breakup
Angular distribution
Near/far decomposition

ABSTRACT

The angular distributions for elastic scattering and breakup of halo nuclei are analysed using a near-side/far-side decomposition within the framework of the dynamical eikonal approximation. This analysis is performed for ^{11}Be impinging on Pb at 69 MeV/nucleon. These distributions exhibit very similar features. In particular they are both near-side dominated, as expected from Coulomb-dominated reactions. The general shape of these distributions is sensitive mostly to the projectile-target interactions, but is also affected by the extension of the halo. This suggests the elastic scattering not to be affected by a loss of flux towards the breakup channel.

1. Introduction

Since their discovery, halo nuclei have been the subject of many theoretical and experimental investigations [1]. These light exotic nuclei exhibit a peculiar quantal structure due to their low separation energy of one or two nucleons. Thanks to this weak binding, these valence nucleons have a significant probability of presence at large distances and form a sort of halo around the core of the nucleus [2]. Since they appear at the edge of the valley of stability, halo nuclei are short-lived and cannot be studied through usual spectroscopic techniques. One usually resorts to reactions to infer information about their structure. Elastic scattering, being a peripheral process, is sensitive mostly to the tail of the wave functions of the colliding nuclei. It may thus be an interesting probe of these exotic nuclei. Moreover, elastic scattering is likely to be affected by reactions, which, like breakup, are significantly enhanced by the weak binding of these nuclei. For that reason, efforts have been made to investigate the effects of the halo upon elastic scattering around the Coulomb barrier [3,4]. These works have shown a significant reduction of the elastic-scattering cross section at large angles compared to stable nuclei. This reduction is interpreted as a loss of flux from the elastic channel towards reaction channels, like breakup or transfer.

Angular distributions for both elastic scattering and breakup are also studied at intermediate energies [5,6]. In Ref. [5], such observables have been measured to evaluate the E2 contribution to the Coulomb breakup of ^{8}B, which is of astrophysical interest. In Ref. [6], angular distributions for the elastic scattering and breakup of ^{11}Be have been measured to investigate the structure of this one-neutron halo nucleus. Both experiments have been successfully reproduced within the dynamical eikonal approximation (DEA) [7–9], which coherently describes both elastic scattering and breakup. Interestingly, the theoretical analysis of the ^{8}B Coulomb breakup has shown significant nuclear-Coulomb interferences that may convey information about the structure of the projectile and/or its interaction with the target [9]. To better understand these features and the interplay between the halo structure and the reaction mechanism, we follow the idea of Ref. [10] and perform a near-side/far-side (N/F) analysis of the DEA angular distributions (see also Ref. [11] for a review). To get a better insight into the influence of breakup onto elastic scattering, we analyse the angular distributions for both processes simultaneously.

We first give a brief account of the DEA and summarise how angular distributions are calculated within this model. We then derive the N/F decomposition of the elastic-scattering cross section and extend that decomposition to angular distributions for elastic breakup. Based on these theoretical developments, we analyse the

* Corresponding author at: National Superconducting Cyclotron Laboratory, Michigan State University, East Lansing, MI 48824, USA.
E-mail addresses: capel@nscl.msu.edu (P. Capel), hussein@if.usp.br (M.S. Hussein), dbaye@ulb.ac.be (D. Baye).
[1] Postdoctoral researcher of the F.R.S.-FNRS.

0370-2693 © 2010 Elsevier B.V. Open access under CC BY license.
doi:10.1016/j.physletb.2010.08.072

elastic scattering and breakup of ^{11}Be, the archetypal one-neutron halo nucleus, on lead at 69 MeV/nucleon, which correspond to the conditions of the RIKEN experiment of Ref. [6].

2. Theoretical considerations

In a nutshell, the DEA [7,8] hinges on using a three-body description of the projectile-target system: The projectile P is seen as a fragment f loosely bound to a core c. This two-cluster structure is described by the internal Hamiltonian H_0, which depends on the c–f relative coordinate $\boldsymbol{r}$ and in which the c–f interaction is simulated by a real potential. The target T is seen as a structureless particle, and its interactions with the core and the fragment are simulated by the optical potentials V_{cT} and V_{fT}. In the DEA, the resulting three-body Schrödinger equation is solved using the eikonal ansatz for the wave function: $\Psi(\boldsymbol{r},\boldsymbol{R}) = e^{iKZ}\widehat{\Psi}(\boldsymbol{r},\boldsymbol{R})$ [12], Z being the component along the beam axis of $\boldsymbol{R}$, the P–T relative coordinate, and $\hbar K$ the initial momentum of the P–T relative motion. At sufficiently high energy, $\widehat{\Psi}$ varies smoothly with $\boldsymbol{R}$, and its second-order derivative in $\boldsymbol{R}$ can be neglected in front of its first-order derivative [12]. This leads to the DEA equation [7,8]

$$i\hbar v\frac{\partial}{\partial Z}\widehat{\Psi}(\boldsymbol{r},\boldsymbol{R}) = (H_0 + V_{cT} + V_{fT} - E_0)\widehat{\Psi}(\boldsymbol{r},\boldsymbol{R}), \tag{1}$$

where v is the initial P velocity, and E_0 the (negative) energy of the projectile ground-state $\phi_{l_0 j_0 m_0}$. The quantum numbers l_0, j_0 and m_0 correspond to the c–f orbital momentum, the projectile total angular momentum and its projection, respectively. The spin of the core being neglected, j_0 is obtained from the coupling of the fragment spin to the orbital momentum. For each value of $\boldsymbol{b}$, the transverse component of $\boldsymbol{R}$, Eq. (1) is solved numerically with the initial condition that the projectile is in its ground state: $\widehat{\Psi}^{(m_0)}(\boldsymbol{r},\boldsymbol{b},Z) \underset{Z\to-\infty}{\longrightarrow} \phi_{l_0 j_0 m_0}(\boldsymbol{r})$.

The transition matrix element for elastic scattering from projection m_0 to m_0' in the direction $\boldsymbol{K} = (K,\theta,\varphi)$ can be obtained from the solutions of (1) [8]

$$T_{\rm el} = 2\pi\hbar v i^{1-|m_0-m_0'|}e^{i(m_0-m_0')\varphi} \times \int_0^\infty b\,db\,J_{|m_0-m_0'|}(qb)S^{(m_0)}_{{\rm el},m_0'}(b), \tag{2}$$

where J_μ is a Bessel function [13], $q = 2K\sin\theta/2$ is the transferred momentum, and the elastic-scattering amplitudes read

$$S^{(m_0)}_{{\rm el},m_0'}(b) = \left\langle \phi_{l_0 j_0 m_0'}(\boldsymbol{r})\middle|\widehat{\Psi}^{(m_0)}(\boldsymbol{r},b\hat{\boldsymbol{X}},Z)\right\rangle_{Z\to+\infty} - \delta_{m_0' m_0}. \tag{3}$$

Following Ref. [10], we divide the $T_{\rm el}$ matrix element (2) into its near (N) and far (F) sides by decomposing the Bessel function into Hankel functions [13]: $J_\mu(z) = \frac{1}{2}[H^{(2)}_\mu(z) + H^{(1)}_\mu(z)]$. The N side corresponds to the expression (2) in which $J_{|m_0-m_0'|}(qb)$ is replaced by $H^{(2)}_{|m_0-m_0'|}(qb)/2$, and the F side to the same expression with $H^{(1)}_{|m_0-m_0'|}(qb)/2$ instead. The N and F sides are related to positive and negative scattering angles, as can be understood from the asymptotic behaviour of the Hankel functions

$$H^{(1)}_\mu(z) \underset{z\to\infty}{\longrightarrow} \sqrt{\frac{2}{\pi z}}e^{\pm i(z-\mu\pi/2-\pi/4)}. \tag{4}$$

Remembering that $q = 2K\sin\theta/2 \approx K\theta$, one sees that the N side arises from positive deflection, while the F side corresponds to negative deflection [10]. The former can thus be interpreted as the contribution of repulsive forces in the P–T scattering, and the latter as resulting from the attractive parts of the P–T interactions. As shown in Refs. [10,11], this decomposition is a powerful tool to analyse reaction mechanisms.

Similarly, a transition matrix can be defined for the dissociation of the projectile [8]. For a final P–T wave vector $\boldsymbol{K'} = (K',\theta,\varphi)$, it reads

$$T_{\rm bu} = 2\pi\hbar v\sum_{ljm} i^{1-|m_0-m|}e^{i(m_0-m)\varphi} \times \int_0^\infty b\,db\,J_{|m_0-m|}(qb)S^{(m_0)}_{\boldsymbol{k}\nu,ljm}(b), \tag{5}$$

whit the transferred momentum $q \approx 2K\sin\theta/2$ and the breakup amplitude

$$S^{(m_0)}_{\boldsymbol{k}\nu,ljm}(b) = \left\langle \chi^{(-)}_{\boldsymbol{k}\nu,ljm}(\boldsymbol{r})\middle|\widehat{\Psi}^{(m_0)}(\boldsymbol{r},b\hat{\boldsymbol{X}},Z)\right\rangle_{Z\to+\infty}. \tag{6}$$

In Eq. (6), $\chi^{(-)}_{\boldsymbol{k}\nu,ljm}$ is the component in the partial wave ljm of the incoming distorted scattering wave $\chi^{(-)}_{\boldsymbol{k}\nu}$ describing the broken-up projectile with a c–f wave vector $\boldsymbol{k}$ and a spin projection ν. These expressions obtained within the DEA enable us to generalise the N/F decomposition to angular distributions for breakup. Using the same decomposition of the Bessel function in Eq. (5), we obtain N and F sides of $T_{\rm bu}$ with the same interpretation.

3. Elastic scattering

We first exploit these theoretical developments by analysing the angular distributions obtained within the DEA for the elastic scattering of ^{11}Be on Pb at 69 MeV/nucleon. This one-neutron halo nucleus is described as a ^{10}Be core in its 0^+ ground state to which a neutron is bound by 0.5 MeV, as explained in Ref. [8]. In that model, the $1/2^+$ ground state is reproduced considering the halo neutron in the $1s_{1/2}$ orbital. We use the optical potentials listed in Ref. [8] to simulate the P–T interactions.

The elastic-scattering cross section, normalised to the Rutherford cross section, is plotted in Fig. 1 as a function of the scattering angle θ (full line). At forward angles, it presents a usual rainbow pattern around the Rutherford cross section. During its drop beyond 2°, the cross section exhibits a second oscillatory pattern. To understand these features, we plot the N and F sides of that cross section. As expected for a reaction dominated by the (repulsive) Coulomb interaction, the elastic-scattering cross section follows its N side at forward angles. It is only at larger angles, after the N side has started to drop, that the F side becomes significant and crosses the N side at about 8°. This crossover explains the second oscillatory pattern as a N/F interference.

The interpretation of the N/F decomposition as positive/negative deflection is based on the asymptotic behaviour of the Hankel functions (4). To assess its validity, we repeat the calculations using the asymptotic expression of the Bessel and Hankel functions. These results, displayed as dotted lines in Fig. 1, are nearly superimposed on the exact expressions, confirming the N/F interpretation.

To evaluate the sensitivity of the pattern of the elastic-scattering cross section to the P–T interactions, the calculation is repeated considering only the Coulomb interaction simulated either by the point–sphere term of the c–T optical potential (PS) or a mere point–point potential between the core and the target (PP). Their dominant N sides are displayed in Fig. 2. We observe two very different results. The PS Coulomb interaction leads to qualitatively similar features as the full optical potential. The PP Coulomb potential, however, leads to a cross section without Coulomb rainbow, very close to Rutherford's. This absence of Coulomb rainbow is

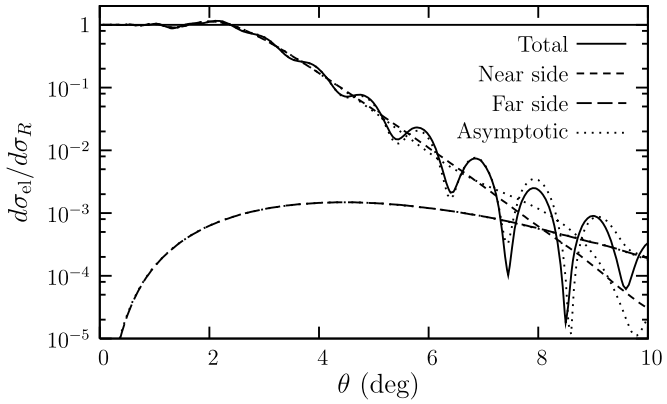

Fig. 1. Elastic-scattering cross section and its N/F decomposition for ^{11}Be impinging on Pb at 69 MeV/nucleon. The results obtained with the asymptotic expression of the Bessel and Hankel functions are shown as dotted lines.

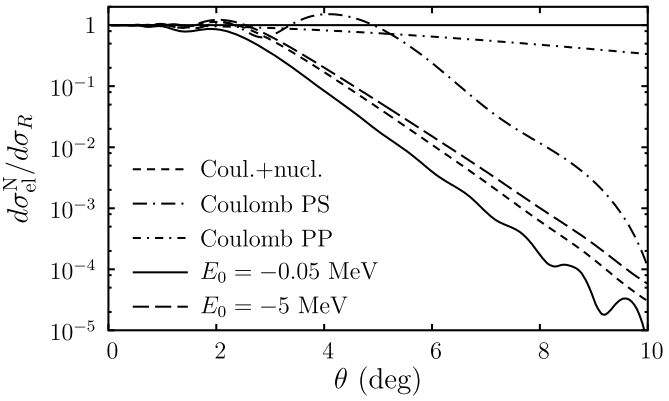

Fig. 2. Influence of the nature of the P–T interactions and of the extension of the halo on the N side of the elastic-scattering cross section of ^{11}Be on Pb at 69 MeV/nucleon.

Table 1
Total breakup and absorption cross sections for three P–T interaction choices and various neutron separation energies.

Interaction	PP	PS	Coulomb + nuclear		
$\lvert E_0\rvert$ (MeV)	0.5	0.5	0.5	0.05	5
$\sigma_{\rm bu}$ (b)	2.58	2.10	1.70	23.57	0.07
$\sigma_{\rm abs}$ (b)	0	0	3.87	4.41	3.58

due to the fact that the PP interaction does not account for the extension of the colliding nuclei, and hence remains quite close to a Coulomb potential between two pointlike particles. On the contrary, the PS calculation, taking account of the finite charge distributions of the core and the target, exhibits a stronger deviation from purely Rutherford scattering.

The inclusion of nuclear optical potentials increases the deviation from the Rutherford cross section. The rainbow pattern hence reflects mostly the nature of the P–T interactions and in particular its deviation from a pure Coulomb potential: the larger the deviation, the smaller the angle at which the drop occurs. Interestingly, it is not related to the loss of flux from the elastic-scattering channel towards the breakup channel. Table 1 displays the total elastic-breakup cross sections $\sigma_{\rm bu}$ obtained in our calculations. We observe that it actually decreases when the deviation from the Rutherford cross section increases. This counterintuitive result suggests that loss from the elastic-scattering channel does not explain the rainbow pattern. A loss of flux is also possible towards the absorption induced by the imaginary part of the optical potentials, which simulates all inelastic processes but breakup. The absorption cross section $\sigma_{\rm abs}$ is also given in Table 1. Since both PP and PS potentials are real, they do not lead to absorption. Therefore, the transfer to this channel cannot explain the rainbow pattern either, confirming that it is mostly sensitive to the P–T interactions. Note that since elastic breakup and absorption include all the inelastic processes simulated within the DEA, the total reaction cross section reads $\sigma_{\rm R} = \sigma_{\rm bu} + \sigma_{\rm abs}$.

To evaluate the sensitivity of the elastic scattering to the extension of the projectile wave function, we perform calculations using ^{11}Be-like projectiles with more extended/compact haloes. This is achieved by varying the binding energy of the ground state from $|E_0| = 0.5$ MeV to 50 keV and 5 MeV. The N sides of the corresponding elastic-scattering cross sections are plotted in Fig. 2. We observe that the N side drops faster as the binding energy decreases, i.e. as the projectile gets more diffuse. The frequency and amplitude of the oscillations before the rainbow, however, remain constant. The sensitivity of the slope of the drop to the projectile extension remains limited, unlike the change in the breakup cross section (see Table 1). This reinforces our idea that breakup does not directly affect elastic scattering. The absorption, though, seems to evolve similarly to the slope of the drop. However, since comparable results are obtained with real nuclear P–T potentials, we conclude that the absorption and the slope of the drop have common roots, i.e. the size of the projectile, but no causal relationship. This study shows that the general features of the elastic-scattering cross section reflect mostly the nature of the P–T interactions, that they are slightly affected by the extension of the projectile, but are not influenced by losses of flux towards other channels.

4. Elastic breakup

We now study in a similar way the angular distribution obtained for the elastic breakup of ^{11}Be on Pb at 69 MeV/nucleon. In Fig. 3, this cross section is plotted for a relative energy $E = 0.5$ MeV between the ^{10}Be core and the neutron after dissociation (full line). Its behaviour is very similar to that of the elastic-scattering cross section: It exhibits a first oscillatory pattern followed by a drop beyond 2°, during which it presents a second set of oscillations. This second set of oscillations is also explained as interferences between the N and F sides.

The calculation of the N/F decomposition of the breakup angular distribution requires a special treatment compared to the elastic scattering. Indeed, both sides diverge at forward angles. This unphysical result is due to the diverging behaviour of the Hankel functions H_μ for $\mu \neq 0$ at small arguments [13]

$$H^{(1)}_{\mu}(z) \underset{z\to 0}{\longrightarrow} \mp\frac{i}{\pi}\Gamma(\mu)(z/2)^{-\mu} \quad \text{for } \mu > 0. \tag{7}$$

This problem can be solved using the asymptotic expression of the Hankel functions (4) down to 0° (dotted lines). This seemingly rough approximation is validated by checking that the angular distribution obtained with the asymptotic expression of the Bessel function is identical to its exact expression. This comparison also confirms the interpretation of the N/F decomposition as positive and negative deflections in elastic breakup.

We observe that the breakup process is also dominated by the N side, and that the oscillatory pattern observed at forward angles and the exponential drop of the cross section beyond 2° are not due to N/F interferences. This similarity with elastic scattering suggests that the forward-angle features are due to a process similar to a Coulomb rainbow. To confirm this idea, we perform calculations with both PS and PP Coulomb interactions and display their N sides in Fig. 3. Again, the PP calculation does not exhibit any oscillation nor sudden drop, as already noted in the DEA calcu-

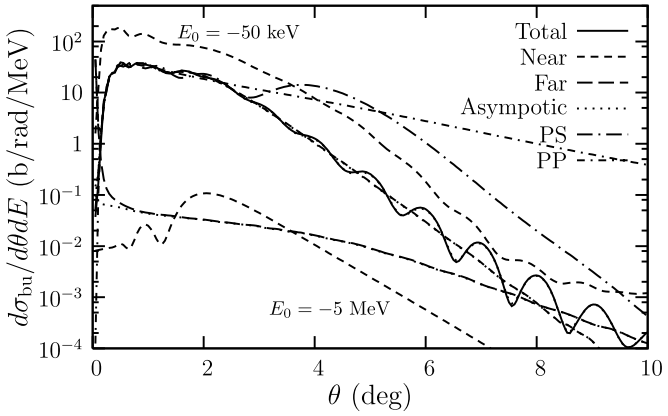

Fig. 3. N/F decomposition of the angular distribution for the elastic breakup of ^{11}Be on Pb at 69 MeV/nucleon for a ^{10}Be-n relative energy $E = 0.5$ MeV. The influence of the nature of the P–T interactions and of the extension of the projectile wave function is also illustrated.

lation of the Coulomb breakup of ^{8}B (see Fig. 7 of Ref. [9]). The PS calculation also exhibits a pattern similar to the Coulomb rainbow observed in elastic scattering. This illustrates that the P–T interactions affect the angular distributions for both elastic scattering and breakup in a similar way, suggesting that the breakup channel does not affect the features of the elastic-scattering cross section.

To complete this study, we repeat our calculations with extended/compacted ^{11}Be-like projectiles. Their N sides, displayed in Fig. 3 (upper and lower dashed curves), confirm the elastic-scattering results, that the slope of the drop of the angular distribution is slightly sensitive to the projectile extension. Note that this conclusion holds although the magnitude of the breakup cross section varies widely with the binding of the projectile, as noted earlier.

5. Conclusion

In this work, we analyse the angular distributions for elastic scattering and breakup using an extension of the N/F decomposition [10,11] applied to the DEA that describes coherently both processes [7,8]. As expected for Coulomb-dominated reactions, we show that the collision of ^{11}Be on Pb at 69 MeV/nucleon is dominated by the N side, i.e. positive deflection, and that N/F interferences are observed only at large scattering angles. The Coulomb-rainbow features are shown to depend mostly on the nature of the P–T interactions, and in particular their deviation from a purely Coulomb potential. We also observe that the slope of the drop in the angular distribution is sensitive to the extension of the projectile wave function. These observations hold for both elastic scattering and breakup.

Examining both elastic scattering and breakup in parallel, this work establishes that the loss of flux towards inelastic channels, like breakup or absorption, does not influence the general features mentioned above. In particular, the slope of the drop of the angular distribution is related to the extension of the projectile, and not to breakup or absorption. Although this sensitivity may be too small to be used as a probe of the halo structure, it can help understanding discrepancies between theoretical predictions and experimental data. In particular, it suggests that the reduction of the cross section for elastic-scattering of halo nuclei around the Coulomb barrier is not due to a loss of flux towards the breakup channel, as proposed in Refs. [3,4], but is more a direct influence of the halo on the collision. To precise this idea, we plan to apply the present methodology, and in particular the parallel study of both elastic scattering and breakup, to low-energy reactions within the continuum discretised coupled channel (CDCC) model [14].

Acknowledgements

This text presents research results of the Belgian Research Initiative on eXotic nuclei (BriX), programme P6/23 on interuniversity attraction poles of the Belgian Federal Science Policy Office. P.C. acknowledges the support of the NSF grant PHY-0800026. He also thanks H. Feldmeier for an interesting discussion on the subject. M.S.H. is supported by the Brazilian agencies CNPq and FAPESP.

References

[1] I. Tanihata, J. Phys. G 22 (1996) 157.
[2] P.G. Hansen, B. Jonson, Europhys. Lett. 4 (1987) 409.
[3] A. Di Pietro, et al., Phys. Rev. C 69 (2004) 044613.
[4] A. Di Pietro, et al., Phys. Rev. Lett. 105 (2010) 022701.
[5] T. Kikuchi, et al., Phys. Lett. B 391 (1997) 261.
[6] N. Fukuda, et al., Phys. Rev. C 70 (2004) 054606.
[7] D. Baye, P. Capel, G. Goldstein, Phys. Rev. Lett. 95 (2005) 082502.
[8] G. Goldstein, D. Baye, P. Capel, Phys. Rev. C 73 (2006) 024602.
[9] G. Goldstein, P. Capel, D. Baye, Phys. Rev. C 76 (2007) 024608.
[10] B.V. Carlson, M.P.I. Filho, M.S. Hussein, Phys. Lett. B 154 (1985) 89.
[11] M.S. Hussein, K.W. McVoy, Prog. Part. Nucl. Phys. 12 (1984) 103.
[12] R.J. Glauber, in: W.E. Brittin, L.G. Dunham (Eds.), Lecture in Theoretical Physics, vol. 1, Interscience, New York, 1959, 315.
[13] M. Abramowitz, I.A. Stegun, Handbook of Mathematical Functions, Dover, New York, 1970.
[14] T. Druet, D. Baye, P. Descouvemont, J.-M. Sparenberg, Nucl. Phys. A 845 (2010) 88.